ACS chemical biology

Articles

pubs.acs.org/acschemicalbiology

Spectroscopic, Molecular Modeling, and NMR-Spectroscopic Investigation of the Binding Mode of the Natural Alkaloids Berberine and Sanguinarine to Human Telomeric G-Quadruplex DNA

Irene Bessi,[†,‡,§] Carla Bazzicalupi,[∥] Christian Richter,[§] Hendrik R. A. Jonker,[§] Krishna Saxena,[§] Claudia Sissi,[⊥] Matteo Chioccioli,[†,‡] Sara Bianco,[⊥] Anna Rita Bilia,[†] Harald Schwalbe,*[,§] and Paola Gratteri*[,†,‡]

[†]Department of Pharmaceutical Sciences and [‡]Laboratory of Molecular Modeling Cheminformatics & QSAR, Department of Pharmaceutical Sciences, University of Firenze, Via Ugo Schiff 6, I-50019 Sesto Fiorentino, Firenze, Italy

[§]Center for Biomolecular Magnetic Resonance, Institute of Organic Chemistry and Chemical Biology, Johann Wolfgang Goethe-University Frankfurt, Max-von-Laue-Strasse 7, 60438 Frankfurt/Main, Germany

[∥]Department of Chemistry "Ugo Schiff", University of Firenze, Via della Lastruccia 3-13, I-50019 Sesto Fiorentino, Firenze, Italy

[⊥]Department of Pharmaceutical Sciences, University of Padova, Via Marzolo 5, 35100 Padova, Italy

Supporting Information

ABSTRACT: G-quadruplex structures can be formed at the single-stranded overhang of telomeric DNA, and ligands able to stabilize this structure have recently been identified as potential anticancer drugs. Among the potential G-quadruplex binders, we have studied the binding ability of berberine and sanguinarine, two members of the alkaloid family, an important class of natural products long known for medicinal purpose. Our spectroscopic (CD, NMR, and fluorescence) studies and molecular modeling approaches revealed binding modes at ligand−complex stoichiometries >1:1 and ligand self-association induced by DNA for the interactions of the natural alkaloids berberine and sanguinarine with the human telomeric G-quadruplex DNA.

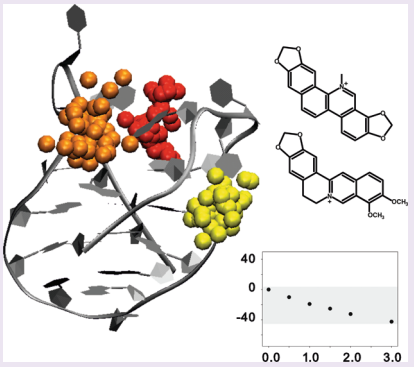

Telomeric DNA and its quadruplex structures are exceptional interesting targets for pharmaceutical intervention.[1−4] Telomeres represent non-coding DNAs located at the end of eukaryotic chromosomes. In human and vertebrate cells they are composed of TTAGGG repeats. The 3′-ends of telomeres are single-stranded and in this form represent the substrate of telomerase, a reverse transcriptase that maintains telomere length homeostasis. Folding of single-stranded telomeric DNA into a G-quadruplex structure prevents hybridization with the telomerase RNA template. Inhibition of telomerase and the related telomere shortening is suggested as a therapeutic selective anticancer strategy. Indeed, telomerase is overexpressed in 80−85% of cancer cells and primary tumors but not in normal somatic cells.[5] On the basis of this evidence, low molecular weight ligands that bind and induce telomeric G-quadruplexes are thus considered potential anticancer drugs, due to their ability to inhibit the activity of the telomerase enzyme resulting from a stabilization of the not properly folded DNA substrate. A number of synthetic compounds have been shown to either stabilize G-quadruplex structures or promote their formation.[5,6] In addition, natural compounds are an important resource for the development of novel drugs with antitumor activity (half of all anticancer drugs internationally approved between 1940 and 2006 are of natural origin). Several features of natural compounds make them very attractive, such as the considerable variability in their chemical structure, their wide availability from natural sources, the low cost of their extraction processes, and most importantly, their general low toxicity.[7]

Up to now, a number of studies have investigated the interaction of G-quadruplexes with small natural compounds.[8−13] Those studies have mainly focused on the planar isoquinoline alkaloid berberine (Scheme 1a) and its derivatives. Additionally, due to its structural similarity to berberine, the benzophenanthridine alkaloid sanguinarine (Scheme 1b) has also been investigated as a potential ligand that is able to promote G-quadruplex folding from human telomeric sequences.[11,14,15]

These compounds with a π-delocalized system and a partial positive charge were found to recognize G-quadruplex structures confirming that they can represent lead structures for further optimization.

Received: July 22, 2011
Accepted: April 9, 2012
Published: April 9, 2012

Scheme 1. Chemical Drawing of (a) Berberine (L1) and (b) Sanguinarine (L2) and Folding Topologies of DNA Telomeric G-Quadruplexes: (c) Basket, (d) Hybrid-1, and (e) Hybrid-2

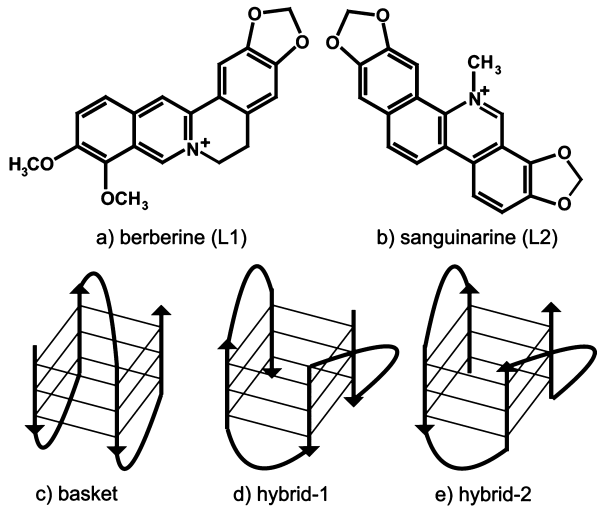

However, to date, structural data are rare, impairing a comprehensive description of the DNA binding mode of these alkaloids. This lack of structural data is likely due to the high structural polymorphism of the human telomeric G-quadruplex DNA in solution. Short human telomeric DNA sequences, containing up to four TTAGGG repeats, are often used as models for structural investigations of the telomere, but very little is known about the biologically relevant fold of long human telomeric DNA *in vivo*.[16,17] Indeed, the G-quadruplex fold depends on several factors, such as flanking nucleotides and nature of stabilizing cation.[18,19] In a Na^+-containing solution, the human telomeric DNA sequence AGGG-$[TTAGGG]_3$ (Tel22) assumes a unique structure, known as basket-type (Scheme 1c),[20] whereas in K^+-containing solution, a mixture of different conformations can coexist.[18] On the other hand, NMR spectroscopy showed that in the presence of K^+, the AAAGGG$[TTAGGG]_3$AA (Tel26) sequence and the TTAGGG$[TTAGGG]_3$TT (wtTel26) sequence, derived from Tel22 by addition of flanking nucleotides, are folded in unique stable arrangements, the hybrid-1 and hybrid-2 topology (Scheme 1d and e), respectively.[21,22]

In the present work, we report a comparison of the binding mode of berberine and sanguinarine to human telomeric G-quadruplex DNA adopting either basket- or hybrid-type fold. The interaction of the two alkaloids with DNA has been investigated by a variety of spectroscopic techniques (fluorescence, CD, and NMR) and molecular modeling approaches. Our investigations show that the natural alkaloids berberine and sanguinarine interact with basket- and hybrid-type human telomeric G-quadruplex DNA with a high stoichiometry as a consequence of specific binding modes and additional ligand self-association induced by DNA binding.

RESULTS

Investigation of the DNA Binding Modes by FRET Melting Studies and CD Binding Studies. The natural ligands L1 or L2 (Scheme 1) have been reported to interact with DNA,[10,11] and to clarify whether they can discriminate between distinct DNA folds, we performed melting experiments detected by fluorescence emission changes in a FRET dye pair on a G-quadruplex forming a sequence resembling the human telomeric sequence (4GGG) as well as on double-stranded DNA (dsDNA) sequences of comparable length. A schematic that shows the principle of the FRET/fluorescence quenching experiment is reported in Supplementary Figure 1. Under the applied experimental conditions (pH 7.4, in the presence of either Na^+ or K^+), the ligands interacted with the G-quadruplex DNA, as indicated by the observed increase of the DNA melting temperature. Binding of L2 induced a larger DNA melting thermal shift than L1. Ligand L2 exhibits a pH-dependent equilibrium between a charged iminium form and a neutral alkanolamine form (with a pK_a of 7.4). Since only the iminium form is known to bind strongly to B-form DNA, we evaluated whether such an equilibrium can affect the DNA recognition by L2 in conditions that are comparable to the physiological one.[23,24] Interestingly, a pH change from 7.0 up to 8.0 did not alter the observed stabilization profile (Supplementary Figure 2).

Both ligands induced only a very small increase in the thermal stability of random dsDNA, when compared to 4GGG (Figures 1 a and b). In particular, for the human telomeric sequence, a higher ΔT_m was observed for the K^+-stabilized G-quadruplex conformations. The melting data showed that L2 induces larger effects on all tested sequences. On the contrary, addition of unlabeled double-stranded DNA to the ligand-bound form of 4GGG displaces preferentially L2 from the G-quadruplex (Supplementary Table 1). Thus, L1 is the most selective binder for the 4GGG telomeric sequence in K^+-containing buffer.

We additionally monitored the DNA−ligand interaction by circular dichroism (CD) spectroscopy (Figure 1 c−f). Comparable changes in the CD spectra were observed upon addition of L1 or L2 to the human telomeric DNA sequence (Tel22) in K^+-containing buffer, suggesting a common binding mode to this hybrid-type G-quadruplex fold.[25] It is noteworthy that in the presence of the telomeric basket-type fold (Na^+-containing buffer), L2 but not L1 caused relevant modifications of the DNA CD spectrum. We cannot exclude that this could be the result of a different binding mode of the two alkaloids on this G-quadruplex structure; however, merged with the melting experiments, it suggests a modest interaction of L1 with the antiparallel basket-type telomeric G-quadruplex.

Equilibrium Binding Studies by Fluorescence. To quantify the binding affinity of L2 toward DNA we performed fluorescence titrations monitoring the fluorescence of the ligand. Accordingly, we monitored L2 binding to the telomeric G-quadruplex DNA (Tel22) folded in either Na^+- or K^+-containing buffer (Supplementary Figure 3) as well as to calf thymus DNA (ctDNA). Data relative to the interaction of L1 with Tel22 in K^+-containing buffer were previously reported,[9,11,26] while in Na^+-containing buffer, the lower binding affinity of L1 to this basket-type fold does not allow a reliable quantitative analysis. Under all conditions, addition of DNA caused quenching of the drug fluorescence signal, which allowed us to determine the binding affinity and the stoichiometry of the complex (Table 1).

Although a preference for G-quadruplexes over ctDNA can be inferred, no large modulation of the binding constant of L2 for different DNA targets was observed. This finding is in agreement with the CD and fluorescence melting data, further confirming the poor selectivity of this compound for a defined DNA arrangement. It is noteworthy that under all of the tested

dx.doi.org/10.1021/cb300096g | ACS Chem. Biol. 2012, 7, 1109−1119

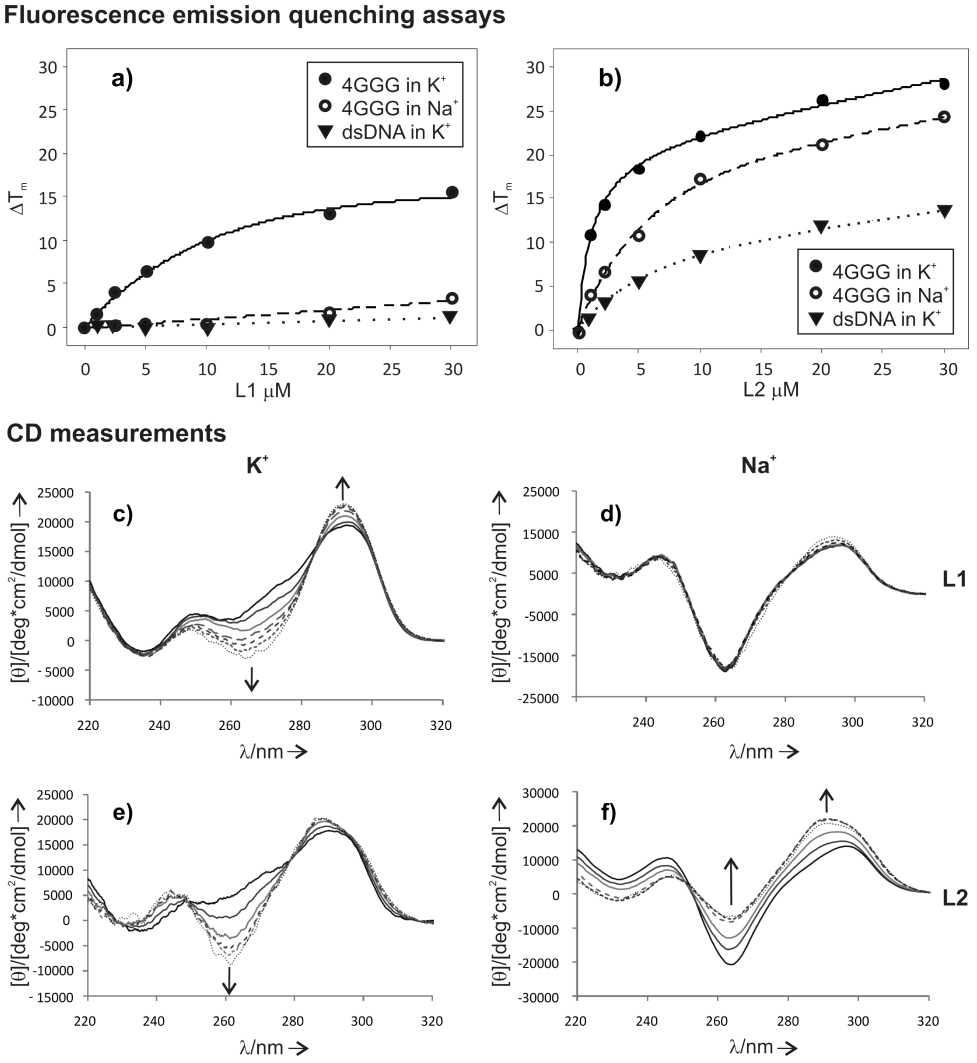

Figure 1. (a, b) Variations of DNA (0.25 μM) melting temperature by increasing concentrations of L1 (a) or L2 (b) in 10 mM LiOH, pH 7.4 with H_3PO_4, 50 mM KCl or NaCl, evaluated by fluorescence melting experiments. Error ±0.4 °C. (●) 4GGG in K^+-containing buffer; (○) 4GGG in Na^+ containing buffer; (▼) dsDNA in K^+-containing buffer. (c–f) Circular dichroism spectra of Tel22 (4 μM) recorded in the presence of increasing L1 (c, d) or L2 (e, f) concentrations (0–50 μM) recorded in 10 mM Tris-HCl, pH 7.5 with 50 mM KCl (c, e) or 50 mM NaCl (d, f).

Table 1. Thermodynamic Parameters from Fluorometric Titrations Performed in 10 mM Tris, pH 7.5 with Added 50 mM NaCl or KCl

target DNA	buffer	$K_b \times 10^6$ (M^{-1})	stoichiometry L2/Tel22	n (bases)[a]
Tel22	K^+	9.14 ± 0.85	2.0 ± 0.1	
	Na^+	2.45 ± 0.21	6.0 ± 0.4	
ctDNA	K^+	1.76 ± 0.15		1.7 ± 0.2

[a]The number of DNA residues involved in the interaction with a single ligand molecule.

conditions a binding stoichiometry higher than 1:1 was detected.

Insights into the Structure of the Complex *via* NMR Spectroscopy and Molecular Modeling. The NMR experiments were planned in order to characterize the interaction of berberine and sanguinarine with antiparallel basket-type as well as hybrid-type folds, which were found to be the prevalent conformations of intramolecular telomeric G-quadruplexes in physiologically relevant conditions.[17]

The experimental conditions and the DNA sequences were chosen to achieve optimal NMR results: the Tel22 sequence was used in Na^+-containing buffer while the Tel26 and wtTel26 sequences were used in K^+-containing buffer. The human telomeric Tel22 sequence AGGG[TTAGGG]$_3$ in Na^+-containing solution forms a unique basket-type structure,[20] while in the presence of K^+, an equilibrium is observed between more hybrid-type structures that are energetically comparable, as indicated by 1D ^{1}H NMR spectra (Supplementary Figures 4 and 5). Simple modifications of the Tel22 sequence lead to a single prevalent structure in K^+-containing solution: the Tel26 sequence AAAGGG[TTAGGG]$_3$AA and the wtTel26 sequence TTAGGG[TTAGGG]$_3$TT are folded into the so-called hybrid-1 and hybrid-2 structures, respectively.[21,22]

The ^{1}H resonances assignment of the ligands (Supplementary Figures 6–9 and Tables 2–3) is in accordance with data reported in the literature.[27,28] The proton resonance assignment for the different DNA folds was performed on the basis of the assignment as previously reported in literature.[20−22] The ^{1}H NMR spectra of Tel22 with assignment of imino region and a ^{31}P NMR proton decoupled spectrum of Tel22 with partial

dx.doi.org/10.1021/cb300096g | ACS Chem. Biol. 2012, 7, 1109–1119

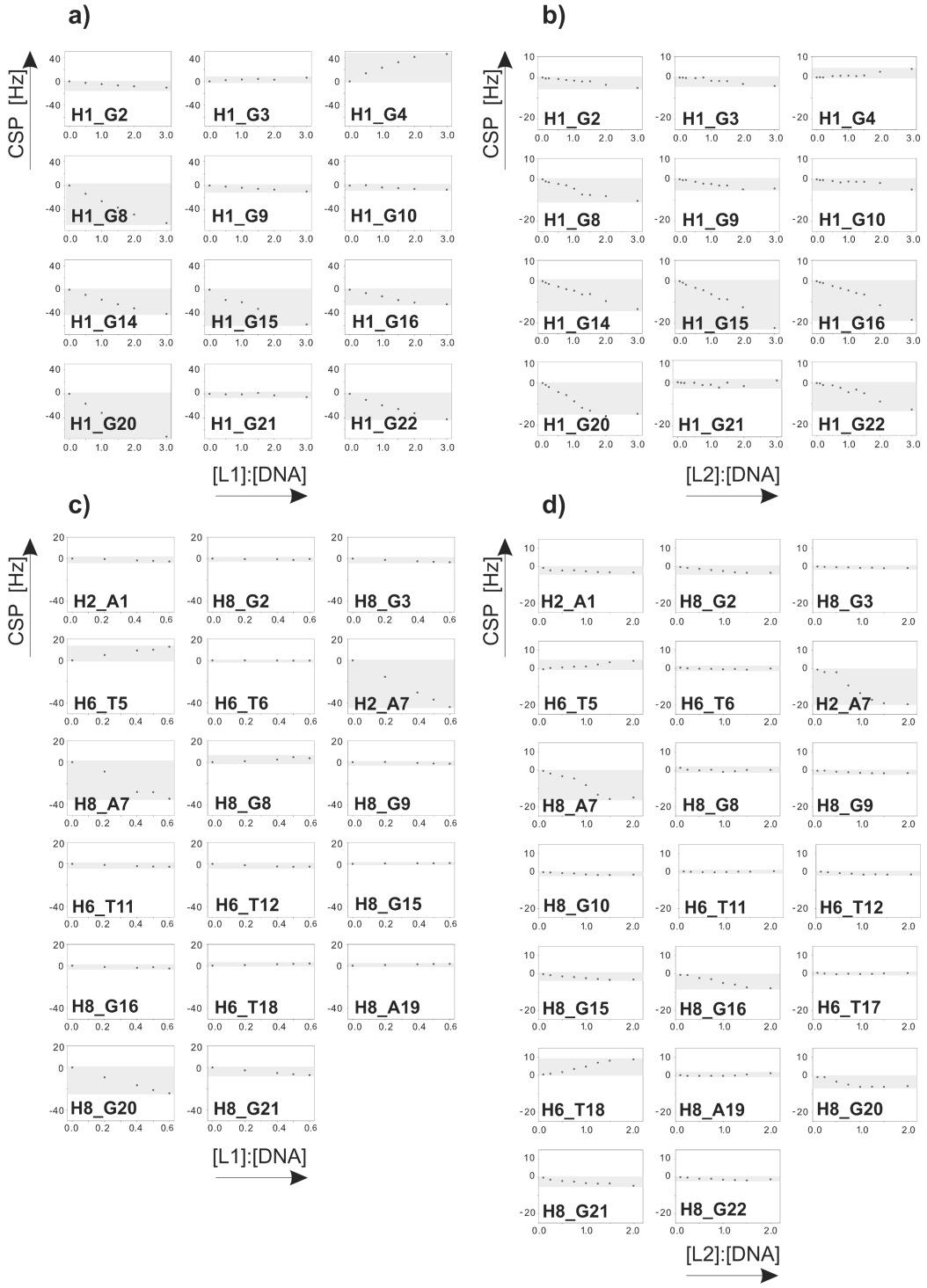

Figure 2. Chemical shift perturbation (CSP) as function of [ligand]:[DNA] molar ratio. (a) CSP of imino protons *versus* [L1]:[DNA]. (b) CSP of imino protons *versus* [L2]:[DNA]. (c) CSP of aromatic protons *versus* [L1]:[DNA]. (d) CSP of aromatic protons *versus* [L2]:[DNA]. (a, c) Titration of L1 up to a [L1]:[DNA] molar ratio equal to 0.6 because the most significant CSP were observed in this range of [L1]:[DNA].

assignment of nucleotides involved in the interaction are included in Supplementary Figures 10−11.

To gain an insight into the binding modes between the ligands and the DNA, NMR titrations of the selected different G-quadruplexes with L1 and L2 were performed. Due to signal overlap, the chemical shift perturbations (CSPs) of Tel26 and wtTel26 could not accurately be monitored (NMR titration data relative to the interaction of berberine with Tel26 and wtTel26 is presented in Supplementary Figure 12), but nevertheless, the broadening of some external G-quartet imino signals can be clearly observed. Therefore, our NMR studies mainly focused on the investigation of the interaction between the ligands and the Tel22 in basket-type conformation.

The CSPs as function of the [ligand]:[DNA] ratio for imino and aromatic proton resonances are displayed in Figure 2.

Imino proton signals that showed the most intense CSP upon addition of L1 are G4, G8, G14-G15-G16, G20, and G22 (Figure 2a). Due to signal overlap in the aromatic region of

dx.doi.org/10.1021/cb300096g | *ACS Chem. Biol.* 2012, 7, 1109−1119

proton spectrum, not all of the aromatic proton chemical shifts could be followed during the titration. G20 (H8) and T5 (H6) are significantly perturbed as well (Figure 2c).

For L2, the most perturbed imino protons belong to the groove defined by the adjacent G14-G15-G16 and G20-G21-G22 stretches, suggesting that this side of Tel22 G-quadruplex should be the one mainly involved in the interaction with L2 (Figure 2b). Among the monitored aromatic protons, A7 (H2, H8) displays a continuous significant resonance shift, up to a saturation level around a molar ratio [L2]:[Tel22] = 1.5; G16 (H8), T18 (H6), and G20 (H8) show relevant induced chemical shifts as well (Figure 2d). For both ligands, an intense broadening of A19 H2 signal can be observed during the titration.

It is noteworthy that the range of chemical shift (cs) variation due to addition of L1 is much larger than that observed upon addition of L2. For example, imino proton of G20 at a ratio ligand:DNA = 3:1 gives rise to a Δcs $\approx$ 15−20 Hz in presence of L2, whereas in presence of L1 the same proton, under the same conditions, is characterized by a Δcs $\approx$ 75 Hz. The extent of the CSP may stem from different effects, such as the different degree of aromaticity of the ligands and thus differences in the induced aromatic ring shifts.

Figure 3 summarizes the chemical shift perturbation data obtained by NMR titrations. On the basis of the ^{1}H CSPs

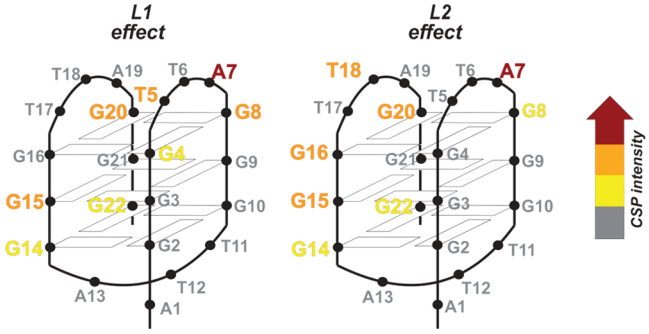

Figure 3. Ligands effect on Tel22 imino and aromatic proton chemical shift derived from NMR titrations in Na^{+}-containing solution.

mapping, the topology of the binding sites is similar for both ligands.

In order to obtain further information concerning the location of the binding sites, proton-decoupled 1D ^{31}P NMR spectra of Tel22 and the Tel22−ligand complexes were recorded. ^{31}P CSPs between the complex and DNA are displayed in Figure 4a. Among the residues that could unambiguously be monitored, phosphates 5 and 17 seem to be most perturbed by L1, whereas in the Tel22:L2 complex, residues 9 and 20 revealed the largest ligand-induced chemical shift perturbation, in accordance with binding regions as indicated by the ^{1}H CSPs.

^{1}H,^{1}H-NOESY and ^{1}H,^{13}C-HSQC spectra were recorded on the Tel22:L2 complex since its higher stability (compared to the Tel22:L1) allowed for longer measurements needed to obtain high quality 2D NMR spectra. ^{1}H,^{1}H-NOESY spectra of the Tel22:L2 complex (Figure 4b) were recorded using different mixing times (100, 300, and 500 ms). The region connecting base aromatic protons with sugar H1′ protons shows that the most shifting peaks involve residues A7, T18, and G20, as already evidenced by NMR titration experiments. Under the applied experimental conditions, no NOE cross peaks between ligand and DNA were observed.

The overlay of the natural abundance 2D ^{1}H,^{13}C-HSQC spectra of free Tel22 with Tel22:L2 complex (Figure 4 c) revealed that the largest chemical shift involves H8−C8 of adenine A1. Furthermore, no signal of the free ligand is detected under the applied experimental conditions. Thus, in order to determine chemical shift perturbations of the ligand and which ligand atoms are mainly involved in the interaction with the G-quadruplex, a titration of L2 upon addition of DNA was performed (Figure 4d). Ligand signals become broader and disappear already at [L2]:[Tel22] ratio of around 30. Precipitation as a potential source for the disappearance of ligand signals was not observed, even after weeks.

Molecular Modeling. Two different modeling approaches were used in this work, a NMR-driven and an unrestrained docking approach. Modeling of the adducts between the ligands and the telomeric DNA in basket-type and hybrid-type conformation was performed using unrestrained docking and validated by NMR-driven docking of L1 and L2 with basket-type DNA. This strategy was chosen because NMR titrations provided unambiguous information only for the quadruplex in basket-type conformation.

Unrestrained Docking: Basket Structure. For the basket-type DNA, the unrestrained docking procedure pointed out three and four interaction sites for L1 and L2, respectively (Figure 5a and b). It is worth noting that two of these binding sites coincide with those observed by NMR-driven docking (orange and yellow color codes in Figure 5). In addition, the A7 adenine residue moves from the original position occupied in the unbound DNA structure and associates *via* H-bond with A19, forming an additional platform available for CH···π or π−π interactions in the case of L1 and L2, respectively (Supplementary Figure 13). The area of the basket-type diagonal loop hosts another interaction site: L1 mainly interacts with the A13 and additionally with G22 *via* CH···π, while L2 is involved in CH···π interaction with A1 (blue molecules in Figure 5a and b. The results obtained for L2 are in agreement with the 2D ^{1}H,^{13}C-HSQC spectral data reported in Figure 4c. In the case of L2, which features a higher stoichiometry ratio than L1, a further localized binding site involves the G8-G9-G19 and G2-G3-G4 stretches (green molecule in Figure 5b).

Unrestrained Docking: Hybrid Structure. An unrestrained docking procedure was used to explore the behavior of both ligands with hybrid-type DNA structures. The lowest energy predicted structures for the ligand−DNA hybrid folding adducts are shown in Figure 5c and d. In the case of L1, the blue ligand is stacked on the 5′-end G-tetrad, interacting *via* π−π stacking with the G10 and *via* CH···π with G4 residues (Supplementary Figure 14). This binding mode is in agreement with the modeling simulation previously reported by Arora *et al.*[9] for the L1:G-quadruplex adduct in K^{+}-containing solution showing the L1 molecule stacked on an external G-quartet. Furthermore, L1 can additionally achieve good π-stacking with the G6 residues from the 3′-end G-tetrad and with A26 (orange molecule in Figure 5c; also Supplementary Figure 14). Moreover, a CH···π interaction is observed with the methyl group of the T7 residue. The results obtained in the case of the complex formed between L2 and the hybrid-type structure are shown in Figure 5d. As observed for the model of L1:DNA hybrid conformation, two poses were found characterized by about 15 kcal/mol energy gap, and in one of them L2 interacts with the 5′-end G-tetrad of the hybrid G-quadruplex (orange

dx.doi.org/10.1021/cb300096g | *ACS Chem. Biol.* 2012, 7, 1109−1119

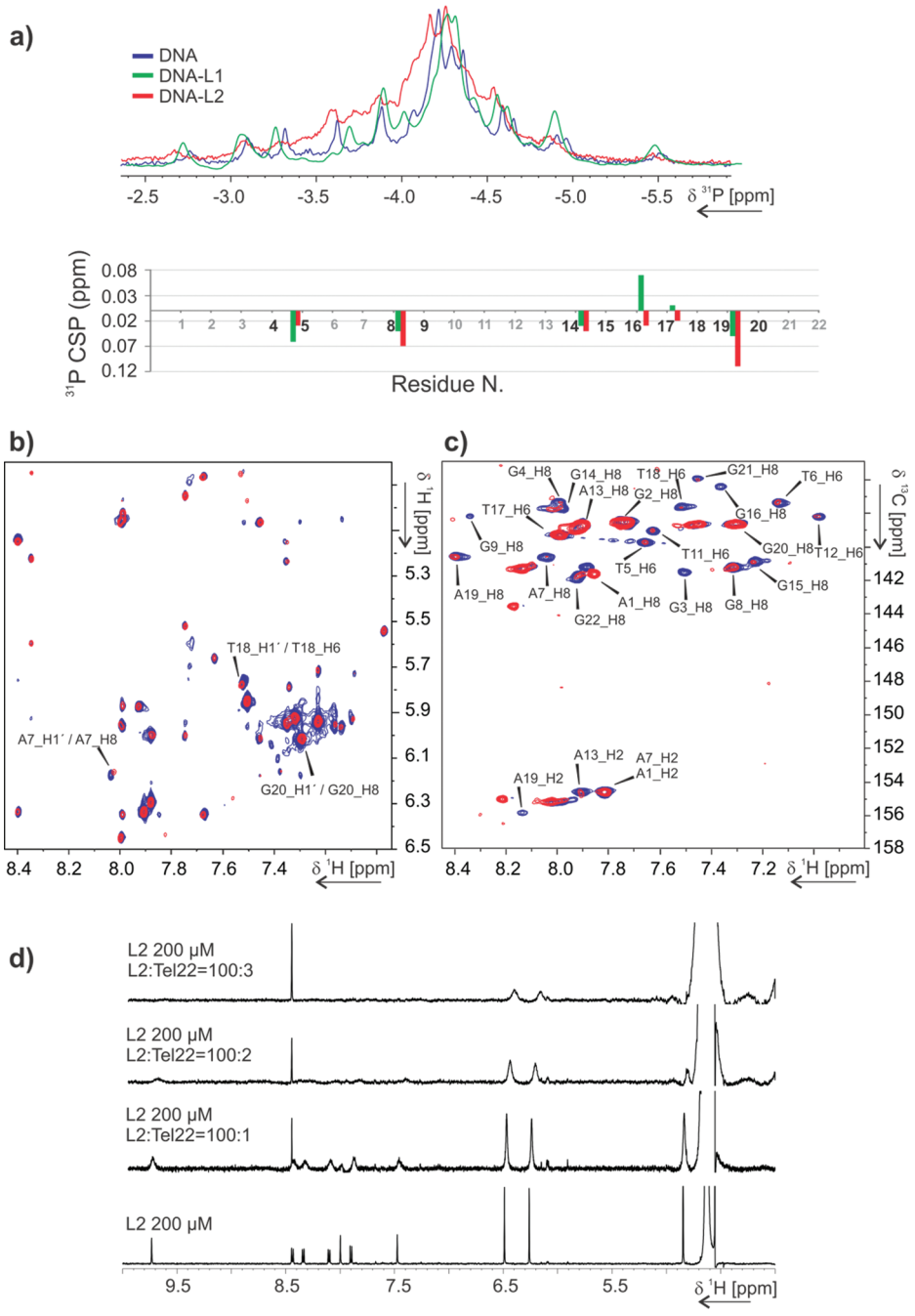

Figure 4. (a) Top: 1D ^{1}H-decoupled ^{31}P NMR spectrum of Tel22:L1 = 1:1.5 complex 200 μM DNA in Na^+-containing buffer, 90% H_2O/10% D_2O, 25 °C, 300 MHz (green) and 1D ^{1}H-decoupled ^{31}P NMR spectrum of Tel22:L2 = 1:2 complex 200 μM DNA in Na^+-containing buffer, 90%H_2O/10% D_2O, 25 °C, 300 MHz (red) overlaid with 1D ^{1}H-decoupled ^{31}P NMR spectrum of Tel22 370 μM in Na^+-containing buffer, 100% D_2O, 25 °C, 300 MHz (blue). Bottom: ^{31}P CSPs due to the ligands are plotted as a function of the residue number N. (b) Overlay of ^{1}H,^{1}H-NOESY of the complex (red, Tel22:L2 = 1:2, Tel22 1 mM, 25 °C, 950 MHz) with the DNA alone (blue, Tel22 370 μM, 25 °C, 600 MHz) in Na^+-containing buffer, 100% D_2O. (c) Overlay of the ^{1}H,^{13}C-HSQC of the complex (red, Tel22:L2 = 1:2, Tel22 300 μM, 25 °C, 700 MHz) with the DNA alone (blue, Tel22 1 mM, 25 °C, 700 MHz) in Na^+-containing buffer, 10% D_2O/90% H_2O. (d) Titration of 200 μM L2 with Tel22 in Na^+-containing buffer 100% D_2O, 37 °C, 700 MHz.

ligand in Figure 5d; also Supplementary Figure 15) and in the other inserts in one lateral groove (yellow ligand in Figure 5d). It is to be noted that the most stable calculated pose for this adduct is the one placed in the groove (yellow molecule, Figure 5d), whereas the other, most likely due to the steric hindrance of the N−CH_3 group, mainly interacts with only one guanine residue of the G-tetrad (orange molecule in Figure 5d).

NMR-Driven Docking. Restrained docking based on NMR data of ligand molecules onto the basket-type G-quadruplex DNA structure clearly indicates the presence of different possible binding sites, in accordance with the hypothesis of multiple binding sites having similar energy derived by spectroscopic titrations. Since NMR titrations did not provide atom specific ligand restraints (since the signals of the ligand are directly lost at the beginning of the titration) and

dx.doi.org/10.1021/cb300096g | *ACS Chem. Biol.* 2012, 7, 1109−1119

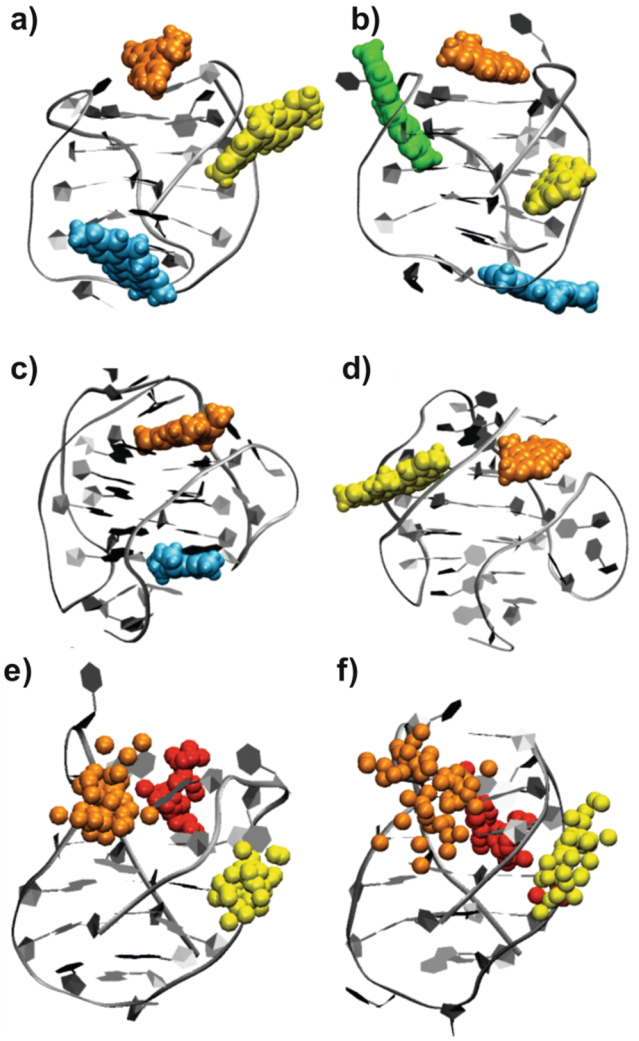

Figure 5. Docking results. Unrestrained-docking poses within 15 kcal/mol from the lowest in energy, obtained for the adducts between L1 and basket-type G-quadruplex DNA (a) and L2 and basket-type G-quadruplex DNA (b). Unrestrained-docking poses within 15 kcal/mol from the lowest in energy, obtained for the adducts between L1 and hybrid-1 type DNA (c) and L2 and hybrid-1 type DNA (d). Overlay of the 50 low-energy representative NMR-driven docking models obtained for the basket-type G-quadruplex DNA with three ligand molecules of the Tel22:L1 complex (e) and the Tel22:L2 complex (f). The ligands are represented as their centroid.

consequently the docking calculations could not produce structures with a unique ligand orientation, only the centroid of each ligand molecule is displayed in Figure 5e and f. The three observed binding sites are similar for both ligands: one binding site is located close to residue A7 (orange centroids in Figure 5e and f), another interaction site is located in the groove defined by G14-G15-G16 and G20-G21-G22 stretches (yellow centroids in Figure 5e and f), and the third binding site (red centroids in Figure 5e and f) is situated either close to the handles of the basket (residues G16-T17 and G4-G3) or toward the G2-G3-G4/G14-G15-G16 groove residues, respectively, for L1 and L2. Two binding sites predicted by unrestrained docking are observed also by NMR-driven docking (orange and yellow color codes in Figure 5). Nevertheless, based on our spectroscopic studies, a higher binding stoichoimetry in the formation of these adducts has to be considered, which may not clearly be monitored by the NMR titrations and which becomes far too ambiguous for NMR-based multiple-ligand docking calculations. The ambiguity raises dramatically as either more binding sites or multiple stacking of ligand molecules in one binding site would be possible.

DISCUSSION

From spectroscopic titrations there is evidence for higher than 1:1 stoichiometry: up to 6 ligand molecules (n) bind to one DNA molecule, depending on the experimental conditions. A different behavior for the two investigated ligands was recently reported that might likely be due to the use of different buffer conditions.[11] Fluorescence data revealed a higher stoichiometry for the basket-type than for the hybrid-type folds (determined in Na^+- or K^+-containing buffer, respectively). We propose that the number of bound molecules determined by fluorescence titration arises from the sum of different energetically similar binding events. Under almost all tested conditions, the complex stoichiometry did not correspond to a simple interaction mode *via* π-stacking with the external G-tetrad, which would most likely involve two ligand molecules per intramolecular telomeric quadruplex. This is remarkably pronounced in the presence of Na^+ where experimental data can be satisfactorily fitted only taking into account a large number of ligands per G-quadruplex unit. A possible explanation might be the formation of unselective interactions corresponding to an external drug binding mode promoted by charge interaction. However, the NMR titration results obtained in Na^+-containing buffer indicate a number of specific binding sites. The overall shape of the 1D ^{31}P NMR spectrum is maintained after adding ligand, and only a limited set of residues is characterized by CSP in the 1D ^1H spectrum, while the others remain clearly unperturbed.

In order to reconcile the experimental findings, we propose the following hypothesis. The binding stoichiomtetry is the result of two different concurring interaction processes: the first involves a number of molecules (n) at least equal to the number of binding sites (m) that specifically interact with the G-quadruplex structure; the latter is the self-association of ligand induced by DNA quadruplex binding and accounts for the remaining interacting molecules ($n - m$).

Self-association of ligand induced by DNA binding is supported by the fact that no signals of free/bound ligand in complex were detected by NMR. In addition, during NMR titration of L2 with Tel22 quadruplex, broadening of ligand signals already occurs at a [ligand]:[DNA] ratio of 100:1 (Figure 4d).

It is noteworthy that a high binding stoichiometry to G-quadruplex structures was previously also observed for porphyrines and was attributed to self-association of the ligand, after binding to G-quadruplex DNA.[29] Most of the small molecules that bind to DNA are planar aromatic compounds of considerable hydrophobic character. Compounds with these properties turn out to be good intercalators and/or minor groove binders but also favor self-association in aqueous solution.[30] The extent of self-association is influenced in particular by the ligand and DNA concentration and by several other factors, such as buffer ionic strength and pH. Therefore this phenomenon cannot be ignored especially when the experimental technique (such as NMR) requires a relatively high concentration.

The binding stoichiometry analysis revealed that the DNA-promoted self-association of L2 is much lower in K^+-containing

buffer (hybrid-type G-quadruplex) than in Na^+-containing buffer (basket-type G-quadruplex). This fact could be explained considering the ligand surface accessibility in the bound state: in the basket-type at least one ligand is observed in an external binding site (orange molecules nearby A7, Figure 5a and 5b), whereas in the case of the complexes with hybrid-type, the ligand surface is less available for further stacking.

The little structural data available frequently refer to a human telomeric quadruplex in propeller-type conformation and present the ligand stacking directly onto the external G-quartets.[31−33] According to our NMR data, we do not find evidence that L1 and L2 stack directly onto the external G-quartets of the basket-type G-quadruplex (Figure 5a and b).

The external G-tetrads in the Tel22 basket-type fold are much more hidden when compared to propeller-type conformation and therefore not so easily accessible for the ligand molecules. Our model suggests that, for the basket-type G-quadruplex fold, the loops and grooves play an important role in ligand recognition.

For both ligands, a higher increase of the melting temperature was observed for the hybrid-type (in K^+-containg buffer) than for the basket-type (in Na^+-containing buffer) fold. Beside the direct metal ion effect on DNA stability, this behavior could reflect a preferred interaction. Ligand L2 appears to be more efficient and L1 more specific in recognizing the different G-quadruplex structure folds. On the basis of our structural results, we can hypothesize that the larger effect on the quadruplex thermal stability observed in K^+-containing solution might be due to the different nature of the binding interactions between ligand and different quadruplex folds. Both L1 and L2 are able to externally stack onto the G-tetrads only when complexed with hybrid-type G-quadruplex structures, whereas for the basket-type structure they can only interact with grooves and loops, mostly *via* π-stacking with the aromatic moiety of a single base.

In summary, our detailed spectroscopic investigations revealed high stoichiometry specific binding modes and additional self-association for the interactions of the natural alkaloids berberine and sanguinarine toward basket-type and hybrid-type human telomeric G-quadruplex DNA. Binding interactions are found to be influenced by several conditions. The multivalent binding and the DNA-induced ligand self-aggregation were not previously described for these ligands and could be used in advanced pharmaceutical anticancer drug research to design analogues with improved specificity to refine the inhibition of the activity of the telomerase enzyme.

METHODS

Material. Berberine and sanguinarine, indicated as L1 and L2, respectively, were purchased from Sigma-Aldrich Co. Ltd. (USA) and used without further purification.

NMR experiments were performed using intramolecular G-quadruplex formed by $d[AG_3(T_2AG_3)_3]$ (Tel22), d[AAAGGG-$(TTAGGG)_3$AA] (Tel26), and $d[TTAGGG(TTAGGG)_3TT]$ (wtTel26), which were purchased by Eurofins MWG Operon (Ebersberg, Germany) as HPSF (High Purity Salt Free) purified oligos and further purified *via* HPLC.

DNA thermal stability was measured by using the sequence 5′ Dabcyl-$AG_3(T_2AG_3)_3$T-FAM 3′ synthesized and purified by ATDBIO (Southampton, U.K.) (4GGG) and the double-stranded fragment (dsDNA) derived from the annealing of the 5′ FAM-GTGAGA-TACCGACAGAAG and CTTCTGTCGGTATCTCAC- Dabcyl 3′ sequences purchased from Eurogentec (Belgium).

Calf thymus DNA (ctDNA) was purchased by Sigma-Aldrich (USA) and used with no further purification.

For fluorescence melting experiments, fluorescence titrations and CD measurements, DNA solutions in the required buffer were heated at 95 °C for 5 min and left to cool at RT overnight. DNA samples used for NMR measurements were prepared using a snap cool annealing procedure in order to avoid the formation of multimers.

Fluorescence Quenching Assays. Fluorescence melting experiments were performed in a Roche LightCycler, using an excitation source at 488 nm. The changes in fluorescence emission were recorded at 520 nm. Melting experiments were performed in a total volume of 20 μL containing 0.25 μM DNA and variable concentrations of tested derivatives in 10 mM LiOH, pH 7.4 with H_3PO_4, and 50 mM KCl or NaCl. Recordings were taken during a heating step from 30 to 95 °C at 1 °C/min.

T_m values were determined from the first derivatives of the melting profiles using the Roche LightCycler software. Each curve was repeated at least three times, and errors were ±0.4 °C.

CD Measurements. Circular dichroism spectra from 200 to 350 nm were recorded at 25 °C using 1 cm path length quartz cells on a Jasco J 810 spectropolarimeter equipped with a NESLAB temperature controller.

CD spectra were recorded on samples containing 4 μM Tel22 and increasing ligands concentrations in 10 mM Tris-HCl, 50 mM KCl or 50 mM NaCl, pH 7.5. The reported spectrum of each sample represents the average of 3 scans. Observed ellipticities were converted to mean residue ellipticity $[\theta]$ = deg × cm^2 × $dmol^{-1}$ (Mol. Ellip.).

Spectrofluorimetric Titration Experiments. Fluorometric titrations were performed at 25 °C in 10 mM Tris-HCl, 50 mM KCl or NaCl, pH 8, with a Perkin-Elmer LS30 fluorometer, equipped with a Haake F3-C thermostat. Binding was followed by addition of increasing amounts of DNA to a freshly prepared drug solution. To avoid large systematic inaccuracies due to experimental errors, the range of bound drug fractions utilized for calculations was 0.15−0.85. All data were analyzed according to Scatchard equation. For ctDNA, data were evaluated according to the equation of McGhee and Von Hippel for non-cooperative ligand−lattice interactions:

$$\frac{r}{m} = \frac{K_b(1 - nr)^n}{[1 - (n - 1)r]^{n-1}} \quad (1)$$

where r is the molar ratio of bound ligand to DNA, m is the free ligand concentration, K_b is the intrinsic binding constant, and n is the exclusion parameter.[34]

NMR Measurements. All NMR samples were referenced with 2,2-dimethyl-2-silapentane-5-sulfonate (DSS) and prepared either in 25 mM Na-phosphate buffer containing 70 mM NaCl (pH = 7.0) or 25 mM K-phosphate buffer containing 70 mM KCl (pH = 7.0). All samples were dissolved in either 90% H_2O/10% D_2O or 100% D_2O. D_2O NMR samples were prepared by repeated freeze-drying and dissolving in D_2O (99.98% D).

The final NMR samples contained 0.015−1 mM DNA or 0.2−0.8 mM ligand in NMR buffer.

NMR spectra of ligands were recorded on Bruker 400 MHz spectrometer at 25 °C. 1D ^1H NMR employed water suppression schemes using excitation sculpting with gradients,[35] and ^1H,^1H-ROESY[36] (200 ms mixing time) and ^1H,^{13}C-HSQC[37−39] experiments were performed for the resonance assignment of the NMR signals of L1 and L2.

NMR spectra of Tel22, Tel22:ligand complexes and NMR titrations were recorded at 25 °C on Bruker 600, 700, 800, 900, and 950 MHz spectrometers.

^1H NMR spectra were recorded on DNA and DNA:ligand complexes with gradient-assisted excitation sculpting for water suppression[35] or jump-return-Echo.[40] ^1H,^{13}C-HSQC[37−39] and 2D ^1H,^1H-NOESY spectra with different water suppression schemes (Watergate[41,42] and excitation sculpting with gradients[35]) and different mixing times (100, 300, and 500 ms) were recorded.

DNA was titrated at 25 °C with ligands up to an excess ratio equal to 3.0 (DNA:ligand). Titration experiments were monitored by 1D ^1H

NMR spectra. 1D ^{31}P NMR spectra were recorded at RT both on Tel22 and Tel22:ligand complex samples on a Bruker 300 MHz spectrometer.

All NMR data were collected, processed, and analyzed using the software TopSpin 2.1 (Bruker) and Sparky 3.[43] The NMR titration curves were made using the software SigmaPlot 11.0.

Molecular Modeling. *Unrestrained Docking.* The binding ability of L1 and L2 (iminium form) has been investigated toward Tel22 basket-type (PDB code: 143D),[20] Tel26 hybrid-1 (PDB code: 2HY9),[21] and wtTel26 hybrid-2 (PDB code: 2JPZ),[22] telomeric G-quadruplex structures. Both ligand molecules have been built by the Build module of Maestro v. 8.5.[44] Docking calculations were performed using Glide v.4.5[45] with the DNA structures kept fixed in their original conformations throughout the docking procedures. Selected poses of the ligand/target (both basket or hybrid fold topologies) complexes were submitted to molecular dynamics simulation for 10 ns in explicit solvent and the root-mean-square deviation (rmsd) of the complexes was monitored *versus* simulation time; 500 cycles of minimization in water implicit solvent treatment (GB/SA) were then applied to all the stable poses (MacroModel, OPLS2005).[46]

The atomic electrostatic charges of the ligands were calculated by means of the RESP procedure,[47] that is, fitting them to an electrostatic potential calculated at the HF/6-31G* level of theory using the Gaussian09 software.[48] Then, general amber force fields (GAFF) parameters were assigned to the ligands by the *antechamber* module implemented in AMBER9 suite.[49] Each complex was immersed in a truncated octahedral box, whose edges were located 10 Å apart from the closest atom of the DNA fragments and contained about 3500 water molecules. To maintain neutrality of the system, 18 Na^+ and 22 K^+ counterions were added to the solvent bulk of the basket-type and of the hybrid-type G-quadruplex−water complexes, respectively. In the case of the basket-type structure, two Na^+ ions were placed along the axis within the central core of the complex, whereas in the case of the hybrid-type structures two K^+ ions were placed along the axis within the central core of the complex, midway between each G-tetrad. Before starting the MD simulations, a minimization of the complexes was performed by setting a convergence criterion on the gradient of 0.01 kcal mol^{-1} Å^{-1}. Then, water shells and counterions were equilibrated for 40 ps at 27 °C, and subsequently, 10 ns of MD simulations in isothermal−isobaric ensemble were performed without any restraint on each complex. The ff03 version of the AMBER force field was used for the DNA fragments and the counterions,[50] whereas the TIP3P model[51] was employed to explicitly represent water molecules. In the production runs, the ligand−DNA fragments systems were simulated under periodic boundary conditions. van der Waals and short-range electrostatic interactions were estimated within a 10 Å cutoff, whereas the long-range electrostatic interactions were assessed by using the particle mesh Ewald method,[52] with 1 Å charge grid spacing interpolated by fourth-order B-spline and by setting the direct sum tolerance to 10^{-5}. Bonds involving hydrogen atoms were constrained by using the SHAKE algorithm[53] with a relative geometric tolerance for coordinate resetting of 0.00001 Å. Berendsen's coupling algorithms[54] were used to maintain constant temperature and pressure with the same scaling factor for both solvent and solutes and with the time constant for heat bath coupling maintained at 1.5 ps. The pressure for the isothermal−isobaric ensemble was regulated by using a pressure relaxation time of 1 ps in the Berendsen's algorithm. The simulations of the solvated complexes were performed using a constant pressure of 1 atm and a constant temperature of 27 °C. A time step of 2 fs was used in the simulations, which were carried out with the AMBER9 program suite.[49]

NMR-Driven Docking. Modeling of the Tel22 basket in complex with the ligands L1 or L2 was achieved using a high ambiguity driven docking approach with the program HADDOCK 2.1.[55,56] The ambiguous interaction restraints (AIRs) were defined from NMR titration experiments for the nucleotides that exhibited significant chemical shift changes upon interaction with the ligand (see Supplementary Tables 4 and 5).

Proton signals that show strong, medium, and weak chemical shift perturbations were restrained to be within a distance of 4.0, 5.0, and 6.0 Å from the ligand(s), respectively. The docking calculations were performed using the coordinates from the NMR structure bundle of the free form DNA quadruplex (PDB code: 143D).[20]

The topology and parameter files for the ligand were manually generated using initial suggestions from the PRODRG server.[57] Furthermore, hydrogen bond restraints have been added (for all except the ones between nucleotides A7-A19, G15-G21, G8-G20 and G20-G16) to keep the secondary structure of the DNA intact during the water refinement. Previous to the docking, arbitrary starting structures were generated from the bundle of 6 DNA structures with up to 4 ligand molecules. In the first iteration, a rigid body docking was performed (7680 structures) starting at 2000 K (500 steps) and cooling down to 500 K (500 steps). Then, semiflexible docking annealing stages were performed in which the semiflexible segments were automatically defined by HADDOCK from 1000 to 50 K (1000 steps) with flexible side-chains at the interface followed by a final annealing stage from 500 to 50 K (1000 steps) with a fully flexible interface. The final lowest energy structures were further refined in explicit water[58] using the nucleic acid forcefield with OPLS charges and Lennard-Jones nonbonded parameters.[59−61] Initial results obtained from docking of 1 and 2 ligand molecules were used to fairly define the binding sites for docking with 3 ligand molecules. The 200 final water-refined docking results were analyzed and clustered (the 3-ligand dockings of berberine and sanguinarine clustered well within a treshold of 5.0 Å and 5.2 Å rmsd, repectively). The top-ranked ensemble, according to the average interaction energy and buried surface area, was accepted as the best representative of the complex.

■ ASSOCIATED CONTENT

Ⓢ Supporting Information

Effect of pH on melting temperature by fluorescence quenching assays; fluorescence titration data; 1D ^{1}H NMR spectra of L1, L2, including proton and carbon resonance assignment; 1D ^{1}H NMR spectra of Tel22 in different experimental conditions; ^{1}H,^{1}H-NOESY of the imino region of Tel22 at different temperatures; 1D ^{31}P NMR spectrum of Tel22, including ^{31}P resonance assignment; titration of Tel26 and wtTel26 monitored by 1D ^{1}H NMR spectra; unrestrained molecular modeling detailed results; definition of ambiguous interaction restraints (AIRs). This material is available free of charge *via* the Internet at http://pubs.acs.org.

■ AUTHOR INFORMATION

Corresponding Author

*E-mail: schwalbe@nmr.uni-frankfurt.de; paola.gratteri@unifi.it.

Notes

The authors declare no competing financial interest.

■ ACKNOWLEDGMENTS

The authors are grateful to the European community (EU-NMR and BIO-NMR). Financial support by the Access to Research Infrastructures activity in the seventh Framework Programme of the EC (Project numbers 261863, Bio-NMR and 261572, WeNMR) for conducting the research is gratefully acknowledged. The state of Hessen (BMRZ) and the Italian Ministero dell'Università e della ricerca are acknowledged for financial support. Ente Cassa di Risparmio di Firenze, Italy is also gratefully acknowledged for a grant to M.C. H.S. is member of the DFG-funded cluster of excellence: macro-molecular complexes.

REFERENCES

(1) Balasubramanian, S., and Neidle, S. (2009) G-quadruplex nucleic acids as therapeutic targets. *Curr. Opin. Chem. Biol. 13*, 345−353.

(2) Ou, T. M., Lu, Y. J., Tan, J. H., Huang, Z. S., Wong, K. Y., and Gu, L. Q. (2008) G-quadruplexes: Targets in anticancer drug design. *ChemMedChem 3*, 690−713.

(3) Neidle, S. (2010) Human telomeric G-quadruplex: The current status of telomeric G-quadruplexes as therapeutic targets in human cancer. *FEBS J. 277*, 1118−1125.

(4) Lipps, H. J., and Rhodes, D. (2009) G-quadruplex structures: in vivo evidence and function. *Trends Cell Biol. 19*, 414−422.

(5) De Cian, A., Lacroix, L., Douarre, C., Temime-Smaali, N., Trentesaux, C., Riou, J. F., and Mergny, J. L. (2008) Targeting telomeres and telomerase. *Biochimie 90*, 131−155.

(6) Arora, A., Kumar, N., Agarwal, T., and Maiti, S. (2010) Human telomeric G-quadruplex: targeting with small molecules (Retraction of vol 6, pg 627, 2008). *FEBS J. 277*, 1345.

(7) Efferth, T., Li, P. C. H., Konkimalla, V. S. B., and Kaina, B. (2007) From traditional Chinese medicine to rational cancer therapy. *Trends Mol. Med. 13*, 353−361.

(8) Franceschin, M., Rossetti, L., D'Ambrosio, A., Schirripa, S., Bianco, A., Ortaggi, G., Savino, M., Schultes, C., and Neidle, S. (2006) Natural and synthetic G-quadruplex interactive berberine derivatives. *Bioorg. Med. Chem. Lett. 16*, 1707−1711.

(9) Arora, A., Balasubramanian, C., Kumar, N., Agrawal, S., Ojha, R. P., and Maiti, S. (2008) Binding of berberine to human telomeric quadruplex - spectroscopic, calorimetric and molecular modeling studies. *FEBS J. 275*, 3971−3983.

(10) Maiti, M., and Kumar, G. S. (2010) Polymorphic nucleic acid binding of bioactive isoquinoline alkaloids and their role in cancer. *J Nucleic Acids 2010*, DOI: 10.4061/2010/593408.

(11) Bhadra, Kakali, and Suresh, K. G. (2011) Interaction of berberine, palmatine, coralyne, and sanguinarine to quadruplex DNA: A comparative spectroscopic and calorimetric study. *Biochim. Biophys. Acta, Gen. Subj. 1810*, 485−496.

(12) Liu, Y. Q., Zheng, B., Xu, X. J., and Yuan, G. (2010) Probing the binding affinity of small-molecule natural products to the G-quadruplex in C-myc oncogene by electrospray ionization mass spectrometry. *Rapid Commun. Mass Spectrom. 24*, 3072−3075.

(13) Li, W., Zhang, M., Zhang, J. L., Li, H. Q., Zhang, X. C., Sun, Q., and Qiu, C. M. (2006) Interactions of daidzin with intramolecular G-quadruplex. *FEBS Lett. 580*, 4905−4910.

(14) Yang, S., Xiang, J., Yang, Q., Zhou, Q., Zhang, X., Li, Q., Tang, Y., and Xu, G. (2010) Distinct G-quadruplex structures of human telomeric DNA formed by the induction of sanguinarine and nitidine under salt-deficient condition. *Fitoterapia 81*, 1026−1032.

(15) Bai, L. P., Hagihara, M., Jiang, Z. H., and Nakatani, K. (2008) Ligand binding to tandem G quadruplexes from human telomeric DNA. *ChemBioChem 9*, 2583−2587.

(16) Petraccone, L., Garbett, N. C., Chaires, J. B., and Trent, J. O. (2010) An integrated molecular dynamics (MD) and experimental study of higher order human telomeric quadruplexes. *Biopolymers 93*, 533−548.

(17) Hänsel, R., Löhr, F., Foldynova-Trantirkova, S., Bamberg, E., Trantirek, L., and Dötsch, V. (2011) The parallel G-quadruplex structure of vertebrate telomeric repeat sequences is not the preferred folding topology under physiological conditions. *Nucleic Acids Res. 39*, 5768−5775.

(18) Dai, J. X., Carver, M., and Yang, D. Z. (2008) Polymorphism of human telomeric quadruplex structures. *Biochimie 90*, 1172−1183.

(19) Phan, A. T. (2010) Human telomeric G-quadruplex: structures of DNA and RNA sequences. *FEBS J. 277*, 1107−1117.

(20) Wang, Y., and Patel, D. J. (1993) Solution structure of the human telomeric repeat D[Ag(3)(T(2)Ag(3))3] G-tetraplex. *Structure 1*, 263−282.

(21) Dai, J. X., Punchihewa, C., Ambrus, A., Chen, D., Jones, R. A., and Yang, D. Z. (2007) Structure of the intramolecular human telomeric G-quadruplex in potassium solution: a novel adenine triple formation. *Nucleic Acids Res. 35*, 2440−2450.

(22) Dai, J. X., Carver, M., Punchihewa, C., Jones, R. A., and Yang, D. Z. (2007) Structure of the Hybrid-2 type intramolecular human telomeric G-quadruplex in K+ solution: insights into structure polymorphism of the human telomeric sequence. *Nucleic Acids Res. 35*, 4927−4940.

(23) Maiti, M., Nandi, R., and Chaudhuri, K. (1983) The effect of Ph on the absorption and fluorescence-spectra of sanguinarine. *Photochem. Photobiol. 38*, 245−249.

(24) Jones, R. R., Harkrader, R. J., and Southard, G. L. (1986) The effect of pH on sanguinarine iminium ion form. *J. Nat. Prod. 49*, 1109−1111.

(25) Zhang, W. J., Ou, T. M., Lu, Y. J., Huang, Y. Y., Wu, W. B., Huang, Z. S., Zhou, J. L., Wong, K. Y., and Gu, L. Q. (2007) 9-Substituted berberine derivatives as G-quadruplex stabilizing ligands in telomeric DNA. *Bioorg. Med. Chem. 15*, 5493−5501.

(26) Maiti, M., and Chaudhuri, K. (1981) Interaction of berberine chloride with naturally occurring deoxyribonucleic acids. *Indian J. Biochem. Biophys. 18*, 245−250.

(27) Tripathi, A. N., Chauhan, L., Thankachan, P. P., and Barthwal, R. (2007) Quantum chemical and nuclear magnetic resonance spectral studies on molecular properties and electronic structure of berberine and berberrubine. *Magn. Reson. Chem. 45*, 647−655.

(28) Marek, R., Tousek, J., Dostal, J., Slavik, J., Dommisse, R., and Sklenar, V. (1999) H-1 and C-13 NMR study of quaternary benzo[*c*]phenanthridine alkaloids. *Magn. Reson. Chem. 37*, 781−787.

(29) Dixon, I. M., Lopez, F., Esteve, J. P., Tejera, A. M., Blasco, M. A., Pratviel, G., and Meunier, B. (2005) Porphyrin derivatives for telomere binding and telomerase inhibition. *ChemBioChem 6*, 123−132.

(30) Buurma, N. J., and Haq, I. (2008) Calorimetric and spectroscopic studies of Hoechst 33258: Self-association and binding to non-cognate DNA. *J. Mol. Biol. 381*, 607−621.

(31) Parkinson, G. N., Ghosh, R., and Neidle, S. (2007) Structural basis for binding of porphyrin to human telomeres. *Biochemistry 46*, 2390−2397.

(32) Parkinson, G. N., Cuenca, F., and Neidle, S. (2008) Topology conservation and loop flexibility in quadruplex-drug recognition: Crystal structures of inter- and intramolecular telomeric DNA quadruplex-drug complexes. *J. Mol. Biol. 381*, 1145−1156.

(33) Campbell, N. H., Parkinson, G. N., Reszka, A. P., and Neidle, S. (2008) Structural basis of DNA quadruplex recognition by an acridine drug. *J. Am. Chem. Soc. 130*, 6722.

(34) McGhee, J. D., and Von Hippel, P. H. (1974) Theoretical aspects of DNA-protein interactions: Co-operative and non-co-operative binding of large ligands to a one-dimensional homogeneous lattice. *J. Mol. Biol. 86*, 469−489.

(35) Hwang, T. L., and Shaka, A. J. (1995) Water suppression that works - Excitation sculpting using arbitrary wave-forms and pulsed-field gradients. *J. Magn. Reson. Ser. A 112*, 275−279.

(36) Bax, A., and Davis, D. G. (1985) Practical aspects of two-dimensional transverse NOE spectroscopy. *J. Magn. Reson. 63*, 207−213.

(37) Schleucher, J., Schwendinger, M., Sattler, M., Schmidt, P., Schedletzky, O., Glaser, S. J., Sorensen, O. W., and Griesinger, C. (1994) A general enhancement scheme in heteronuclear multidimensional NMR employing pulsed-field gradients. *J. Biomol. NMR 4*, 301−306.

(38) Kay, L. E., Keifer, P., and Saarinen, T. (1992) Pure absorption gradient enhanced heteronuclear single quantum correlation spectroscopy with improved sensitivity. *J. Am. Chem. Soc. 114*, 10663−10665.

(39) Palmer, A. G., Cavanagh, J., Wright, P. E., and Rance, M. (1991) Sensitivity improvement in proton-detected 2-dimensional heteronuclear correlation NMR-spectroscopy. *J. Magn. Reson. 93*, 151−170.

(40) Sklenar, V., and Bax, A. (1987) Spin-Echo water suppression for the generation of pure-phase two-dimensional NMR-spectra. *J. Magn. Reson. 74*, 469.

(41) Piotto, M., Saudek, V., and Sklenar, V. (1992) Gradient-Tailored Excitation for Single-Quantum NMR-Spectroscopy of Aqueous-Solutions. *J. Biomol. NMR 2*, 661−666.

(42) Sklenar, V., Piotto, M., Leppik, R., and Saudek, V. (1993) Gradient-Tailored Water Suppression for ^{1}H-^{15}N HSQC Experiments Optimized to Retain Full Sensitivity. *J. Magn. Reson. Ser. A 102*, 241−245.
(43) Goddard, T. D., Kneller, D. G. (2007) *SPARKY 3*, University of California, San Francisco.
(44) *Maestro v 8.5* (2007) Schrödinger, LLC, New York, NY.
(45) *Glide v. 4.5* (2007) Schrödinger, LLC, New York, NY.
(46) *Macromodel v. 9.6* (2008) Schrödinger, L.L.C., New York, NY.
(47) Bayly, C. I., Cieplak, P., Cornell, W. D., and Kollman, P. A. (1993) A well-behaved electrostatic potential based method using charge restraints for deriving atomic charges - the Resp model. *J. Phys. Chem. 97*, 10269−10280.
(48) Frisch, M. J., Trucks, G. W., Schlegel, H. B., Scuseria, G. E., Robb, M. A., Cheeseman, J. R., Scalmani, G., Barone, V., Mennucci, B., Petersson, G. A., Nakatsuji, H., Caricato, M., Li, X., Hratchian, H. P., Izmaylov, A. F., Bloino, J., Zheng, G., Sonnenberg, J. L., Hada, M., Ehara, M., Toyota, K., Fukuda, R., Hasegawa, J., Ishida, M., Nakajima, T., Honda, Y., Kitao, O., Nakai, H., Vreven, T., Montgomery Jr., J. A., Peralta, J. E., Ogliaro, F., Bearpark, M., Heyd, J. J., Brothers, E., Kudin, K. N., Staroverov, V. N., Kobayashi, R., Normand, J., Raghavachari, K., Rendell, A., Burant, J. C., Iyengar, S. S., Tomasi, J., Cossi, M., Rega, N., Millam, J. M., Klene, M., Knox, J. E., Cross, J. B., Bakken, V., Adamo, C., Jaramillo, J., Gomperts, R., Stratmann, R. E., Yazyev, O., Austin, A. J., Cammi, R., Pomelli, C., Ochterski, J. W., Martin, R. L., Morokuma, K., Zakrzewski, V. G., Voth, G. A., Salvador, P., Dannenberg, J. J., Dapprich, S., Daniels, A. D., Farkas, Ö., Foresman, J. B., Ortiz, J. V., Cioslowski, J., and Fox, D. J. (2009) *Gaussian 09*, Revision A.01 ed., Gaussian, Inc., Wallingford, CT.
(49) Case, D. A., Darden, T. A., Cheatham, T. E., III, Simmerling, C. L., Wang, J., Duke, R. E., Luo, R., Merz, K. M., Pearlman, D. A., Crowley, M., Walker, R. C., Zhang, W., Wang, B., Hayik, S., Roitberg, A., Seabra, G., Wong, K. F., Paesani, F., Wu, X., Brozell, S., Tsui, V., Gohlke, H., Yang, L., Tan, C., Mongan, J., Hornak, V., Cui, G., Beroza, P., Mathews, D. H., Schafmeister, C., Ross, W. S., and Kollman, P. A. (2006) *AMBER 9*, University of California, San Francisco, CA.
(50) Duan, Y., Wu, C., Chowdhury, S., Lee, M. C., Xiong, G. M., Zhang, W., Yang, R., Cieplak, P., Luo, R., Lee, T., Caldwell, J., Wang, J. M., and Kollman, P. (2003) A point-charge force field for molecular mechanics simulations of proteins based on condensed-phase quantum mechanical calculations. *J. Comput. Chem. 24*, 1999−2012.
(51) Jorgensen, W. L., Chandrasekhar, J., Madura, J. D., Impey, R. W., and Klein, M. L. (1983) Comparison of simple potential functions for simulating liquid water. *J. Chem. Phys. 79*, 926−935.
(52) Essmann, U., Perera, L., Berkowitz, M. L., Darden, T., Lee, H., and Pedersen, L. G. (1995) A smooth particle mesh Ewald method. *J. Chem. Phys. 103*, 8577−8593.
(53) Ryckaert, J. P., Ciccotti, G., and Berendsen, H. J. C. (1977) Numerical-integration of cartesian equations of motion of a system with constraints - molecular-dynamics of N-alkanes. *J. Comput. Phys. 23*, 327−341.
(54) Berendsen, H. J. C., Postma, J. P. M, van Gunsteren, W. F., Dinola, A., and Haak, J. R. (1984) Molecular-dynamics with coupling to an external bath. *J. Chem. Phys. 81*, 3684−3690.
(55) Dominguez, C., Boelens, R., and Bonvin, A. M. J. J. (2003) HADDOCK: A protein-protein docking approach based on biochemical or biophysical information. *J. Am. Chem. Soc. 125*, 1731−1737.
(56) van Dijk, M., van Dijk, A. D. J., Hsu, V., Boelens, R., and Bonvin, A. M. J. J. (2006) Information-driven protein-DNA docking using HADDOCK: it is a matter of flexibility. *Nucleic Acids Res. 34*, 3317−3325.
(57) Schüttelkopf, A. W., and van Aalten, D. M. F. (2004) PRODRG: a tool for high-throughput crystallography of protein-ligand complexes. *Acta Crystallogr., Sect. D: Biol. Crystallogr. 60*, 1355−1363.
(58) Linge, J. P., Williams, M. A., Spronk, C. A. E. M., Bonvin, A. M. J. J., and Nilges, M. (2003) Refinement of protein structures in explicit solvent. *Proteins: Struct., Funct., Bioinf, 50*, 496−506.
(59) Jorgensen, W. L., and Tirado-Rives, J. (1988) The OPLS force field for proteins. energy minimizations for crystals of cyclic peptides and crambin. *J. Am. Chem. Soc. 110*, 1657−1666.
(60) Pranata, J., Wierschke, S. G., and Jorgensen, W. L. (1991) OPLS potential functions for nucleotide bases - relative association constants of hydrogen-bonded base-pairs in chloroform. *J. Am. Chem. Soc. 113*, 2810−2819.
(61) Nozinovic, S., Fürtig, B., Jonker, H. R. A., Richter, C., and Schwalbe, H. (2010) High-resolution NMR structure of an RNA model system: the 14-mer cUUCGg tetraloop hairpin RNA. *Nucleic Acids Res. 38*, 683−694.